

# Preparation of the calibration unit for LINC-NIRVANA

Lucas Labadie<sup>a</sup>, Fulvio de Bonis<sup>a</sup>, Sebastian Egner<sup>a</sup>, Tom Herbst<sup>a</sup>, Peter Bizenberger<sup>a</sup>, Martin Kürster<sup>a</sup>, Alain Delboulé<sup>b</sup>

<sup>a</sup> Max-Planck Institut für Astronomie, Königstuhl, 17, D-69117 Heidelberg, Germany;

<sup>b</sup> Laboratoire d'Astrophysique de Grenoble, BP 53, F-38041 Grenoble Cedex 9, France;

## ABSTRACT

We present in this paper the status of the calibration unit for the interferometric infrared imager LINC-NIRVANA that will be installed on the Large Binocular Telescope, Arizona. LINC-NIRVANA will combine high angular resolution ( $\sim 10$  mas in J), and wide field-of-view (up to  $2' \times 2'$ ) thanks to the conjunct use of interferometry and MCAO. The goal of the calibration unit is to provide calibration tools for the different sub-systems of the instrument. We give an overview of the different tasks that are foreseen as well as of the preliminary detailed design. We show some interferometric results obtained with specific fiber splitters optimized for LINC-NIRVANA. The different components of the calibration unit will be used either during the integration phase on site, or during the science exploitation phase of the instrument.

**Keywords:** Infrared interferometry, infrared instrumentation, fibers, instrument calibration

## 1. INTRODUCTION

LINC-NIRVANA is the wide-field near-infrared imager of the Large Binocular Telescope, a unique facility installed on Mount Graham, Arizona, which will become fully operational in 2009. The LBT is composed of two 8.4-m telescopes jointly moved by an alt-azimuth mount. They are separated by 14.4 meters center-to-center and constitute the aperture for the two interferometers of the observatory, LINC-NIRVANA and the LBTI. Beside these two instruments, each eye feeds several optical/infrared imagers and/or spectrographs (LBC Blue and Red, LUCIFER...), making the LBT a compact observatory hosting at least 10 instruments.

LINC-NIRVANA is a near-infrared interferometer working in the J, H and K bands for which the two beams are combined in the image-plane, in the so-called Fizeau mode. When the output pupil remains a scaled version of the interferometer input pupil – the “pupil homotheticity” condition –, the field-of-view is preserved and any point-like source in the FOV appears as a fringed point-spread function. This results in angular resolution along the baseline equivalent to a 23-m telescope, i.e. an unprecedented resolution for a ground-based direct imager. In order to take advantage of the large FOV capabilities of the Fizeau scheme, the atmospheric turbulence must also be corrected over a similar scale, which is achieved by the Multi-Conjugated Adaptive Optics system (MCAO) of LINC-NIRVANA. For the first time, LINC-NIRVANA will combine two advanced techniques like interferometry and MCAO to reach a resolution of 20 mas in K over a field-of-view up to  $2' \times 2'$ .

Operating LINC-NIRVANA also requires to develop calibration tools, techniques and strategy to periodically adjust the instrument, considering its science objectives. Calibration operations are divided into those necessary during the AIT (Assembly, Integration and Testing) phase and those that will be used on-sky on a regular basis during the lifetime of the instrument. Within these categories, the calibration tasks must include operations related to the interferometric beam combiner, to the Multi-Conjugated AO, to the detector flat fields as well as to the non-common path aberrations between the science channel and the wavefront sensor channel.

## 2. SYSTEM OVERVIEW

We briefly describe the different sub-systems of the instrument. More details on each of these aspects can be found in other papers of this conference.

---

Further author information: (Send correspondence to Lucas Labadie)

Lucas Labadie: E-mail: labadie@mpia.de, Telephone: +49 (0)6221 52 82 39

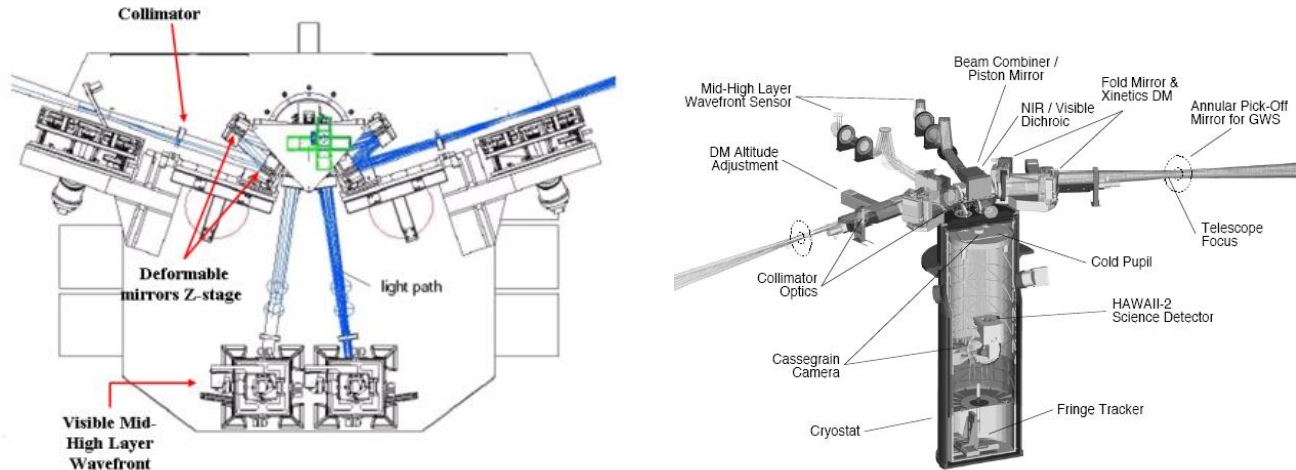


**Figure 1.** Top view and 3D view of the LINC-NIRVANA bench. *Left:* The visible channel of each arm feeds the mid-high layer wavefront sensor. *Right:* The piston mirror launches the science beams into the cryostat, which lies vertically under the bench.

Each eye of the LBT feeds LINC-NIRVANA which lies on the fixed platform between the two primary mirrors. The F/15 beam arriving from the telescope focal plane enters the multi-lens collimator. This sub-system first achieves a quasi collimation of the beam in order to optimize the coverage of the DM-mirrors that constitute the z-stage. The true collimation is performed afterwards using a third lens in the fore-optics group. The two collimated beams are then redirected at 45° into the cryostat using the piston-mirror, which is also a key component of the fringe-tracking system. The cold pupil is placed right after the cryostat entrance window, improving the infrared performance. The beams are combined inside the cryostat on the infrared detector. An infrared dichroic filter wheel allows us to select a specific band in the NIR spectrum. The rest of the light continues through the channel reserved and reaches the fringe tracking unit.

The detector is a Rockwell 2k×2k with a 5 mas pixel scale. The science field-of-view is then limited by the detector to 10"×10" for a given exposure. The sky rotates with respect to the entrance pupil – and therefore to the detector – due to the alt-azimuthal nature of the telescope. We use a field derotator as a classical solution to compensate this effect and to afford longer exposure time. On the other hand, the fringes remains always fixed with respect to the baseline (i.e. the entrance pupil), and if the detector rotates the fringe pattern will cover different position angles during the night. This is a valuable effect in terms of *uv* coverage, although it can result in contrast loss within a single exposure. Simulations have shown that even for integration times of several minutes, the blurring of the fringes remains acceptable.

The fringe tracking system operates in the infrared band not used for the science observations. This system measures the fringe contrast on a reference star within a 1.5'×1' field-of-view and controls the piston-mirror to correct for the residual OPD. The piston mirror travel range is ±75 μm at a frequency up to 200 Hz.

Before entering the cryostat, the two beams pass through a dichroic splitter that splits the light into the infrared science channel and a visible channel. The last one feeds the Mid-High Layer Wavefront Sensors that provide the wide-field correction of the atmospheric turbulence.

### 3. THE ROLE OF THE CALIBRATION UNIT

The calibration unit is responsible for providing calibration tools for the following instrument sub-systems or for specific perturbations:

- The Multi-Conjugate Adaptive Optics system for the correction of the atmospheric turbulence over a large

field-of-view. In LINC-NIRVANA, the Mid-High Layer Wavefront Sensors are coupled with the deformable mirrors conjugated to the mid ( $\sim 4$  km) or high ( $\sim 12$  km) atmospheric layers. The MHWS uses eight pyramid wavefront sensors that move inside the 2 arcmin field-of-view and pick up bright reference stars for wavefront sensing.

- The piston mirror, which is responsible for the fast tracking of the differential OPD in combination with the Fringe and Flexure Tracking (FFT) system located in the cryostat.
- The different optical train between the visible MHWS channel and the science channel results in static *non-common path aberrations* (NCPA). A wavefront error attributed to any degradation within the common AO loop is seen in the same way in the wavefront sensor and in the science detector channels, allowing us an efficient correction. At the opposite, the wavefront errors due to optical components outside the AO loop are not observed in the science channel. This bias has to be calibrated in order to allow a proper AO correction.

### 3.1. Phase Diversity

This bias can be properly calibrated using a method such as the *Phase Diversity* (PD) that can sense the wavefront in the science channel down to the detector. The PD is a curvature sensing method that consists in introducing a known aberration – typically a defocus – leaving any other setting unchanged<sup>1,2</sup>. The *in focus* and *out of focus* images are then compared through a criterion minimization algorithm from which the Zernike spectrum is extracted. This corresponds to *static* aberrations outside the AO-loop that have to be taken into account in a look-up table for the wavefront sensor.

Fig 2 shows the principle of phase diversity. An unresolved source is imaged on the detector giving the *in focus* position. The detector is then shifted in order to obtain two *out of focus* images of the source. At a given wavelength, the relation between the resulting phase shift  $\Delta\phi$  and the applied linear displacement  $d$  is

$$\Delta\phi = \frac{\pi d}{4\lambda(F/D)^2} \quad (1)$$

where  $F/D$  is the numerical aperture of the beam. To achieve an optical accuracy with this method, the applied phase shift should be between  $\pi$  and  $3\pi$ . However, moving the detector itself can be a critical operation because the slow beams ( $F/80$ ) require a high displacement  $d$  of the detector to reach the required phase shift, which is not possible in the case of LINC-NIRVANA.

Thus, rather than moving the detector in the image plane, we plan to move the point-like source at the telescope focus. Considering that LINC-NIRVANA has a beam aperture of  $F/15$  at the telescope focus, the required displacement is  $\sim 2.5$  mm. This option is already in use for the calibration of static errors on NACO/VLT. It should be noted that defocusing by moving an object in the entrance focal plane or by shifting the detector is not strictly equivalent. However, it has been shown theoretically that this differential effect is negligible.<sup>3</sup>

In our setup, the point-like source is obtained by placing at the telescope focus a single-mode fiber that can be

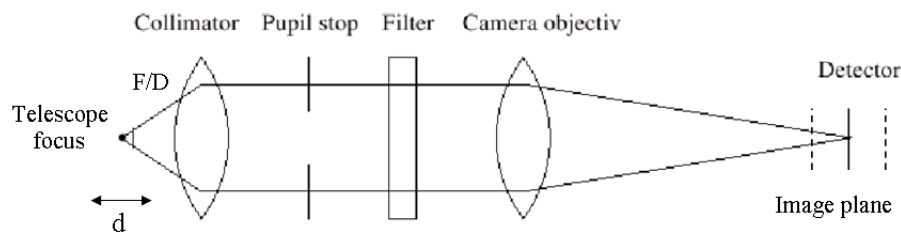


**Figure 2.** Principle of phase diversity (from Hartung et al. 2003). In the detector plane, the continuous line represent the *in focus* position, while the dashed line represent the *out of focus* positions.

moved by the necessary amount, if placed on a translation stage. A second option is to use a fiber splitter with one input and three outputs for which one fiber corresponds to the *in focus* position and the two other fibers to the respective positions  $\pm 2.5$  mm as shown in Fig. 3.

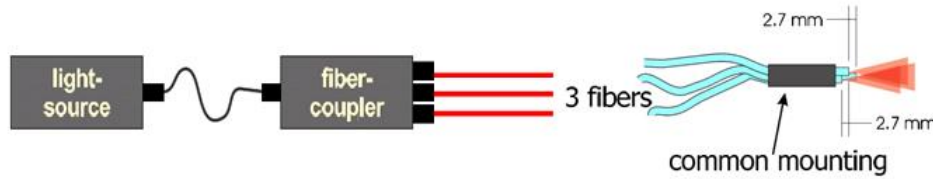


**Figure 3.** Mounting for the phase diversity.

The advantage of the last option is to get a simultaneous acquisition of the in focus and out of focus images, which guarantees always the same relative displacement and thus the same phase shift. However, the three different images will not correspond to an identical optical path due to their relative transverse shift, leading to potential inaccuracies. Although this effect should be negligible, this still needs to be assessed experimentally in the lab. We also decided to keep the phase diversity unit on a translation stage in focus in order to ensure the possibility to switch between the two presented options.

### 3.2. Interferometric calibration

To achieve interferometric beam combination, the optical paths in the two arms of the instrument have to fulfill a certain number of requirements. In particular, three aspects have to be considered:

- Verify the internal zero optical path difference between the two telescope foci
- Verify the homotheticity of the pupil (pupil position, pupil size, focal length of the collimator)
- Check the position of the optical axis

#### 3.2.1. Verification of the internal zero optical path difference

For the calibration of the zero OPD between the two arms, we propose to use two coherent artificial stars placed in the focal plane of the telescope. These sources must have theoretically zero relative OPD in order to be used as references. A possible solution is to use a fiber splitters with one input and two outputs, each output simulating a star at the telescope focus. Practically, the splitter arms must be equalized down to  $\sim 20 \mu\text{m}$  (limited by the  $\pm 75 \mu\text{m}$  dynamic range of the piston mirror). Hence, the fiber splitter will simulate a coherent source that can be tracked by the piston mirror. If this last unit is placed at its zero nominal position, the collimator groups can be re-aligned until fringes are found. The zero-OPD sub-system is placed on-axis.

#### 3.2.2. Homotheticity verification

Pupil misalignment (position, size) can affect the homotheticity conditions and prevent us from obtaining fringes over the whole field-of-view in the Fizeau recombination scheme. Thus, once the on-axis zero-OPD is ensured, we foresee to use an off-axis coherent source placed at the telescope focus as well to simultaneously verify that fringes can be obtained on-axis and off-axis. This is a key verification of the pupil homotheticity that strongly influences the proper operation of the instrument as a Fizeau interferometer.

### 3.3. Mid-High Wavefront Sensor calibration

Another key sub-system for LINC-NIRVANA is obviously the system of Multi Conjugated Adaptive Optics installed in the two arms of the interferometer and that permits to deliver a correction of the atmospheric turbulence over a field of view sufficiently large to consider LINC-NIRVANA as a wide field imager. The calibration of the MCAO system includes the calibration of the deformable mirrors (the Xinetics DMs) and the wavefront-sensor. The Mid-High Layer Wavefront Sensor (MHWS) senses the turbulent layer at two different altitudes,  $\sim 4$  km and  $\sim 10$  km, defined respectively as the mid and high layers at which the DMs are optically conjugated.

Three operations are foreseen:

- Flattening of the Xinetics deformable mirrors
- Recovering of the Gradient Matrix
- Calibrating the linear stages.

These various operations can be achieved in practice by simulating a stellar field in the focal plane of the telescope (see Sect. 4.1)

## 4. THE DESIGN OF THE CALIBRATION UNIT

The calibration unit acts as a reference for the operation of the different instrument sub-units and for the alignment along optical axis. The design concept is driven by the strong requirement of a light and stiff unit almost insensitive to flexure while tilting the bench.

The design of the calibration unit is shown in Fig. 4. The system is based on four components fixed in circle at specified positions corresponding to the telescope focus. Any of these components can feed the instrument thanks to a rotating flat mirror that picks up the desired beam.

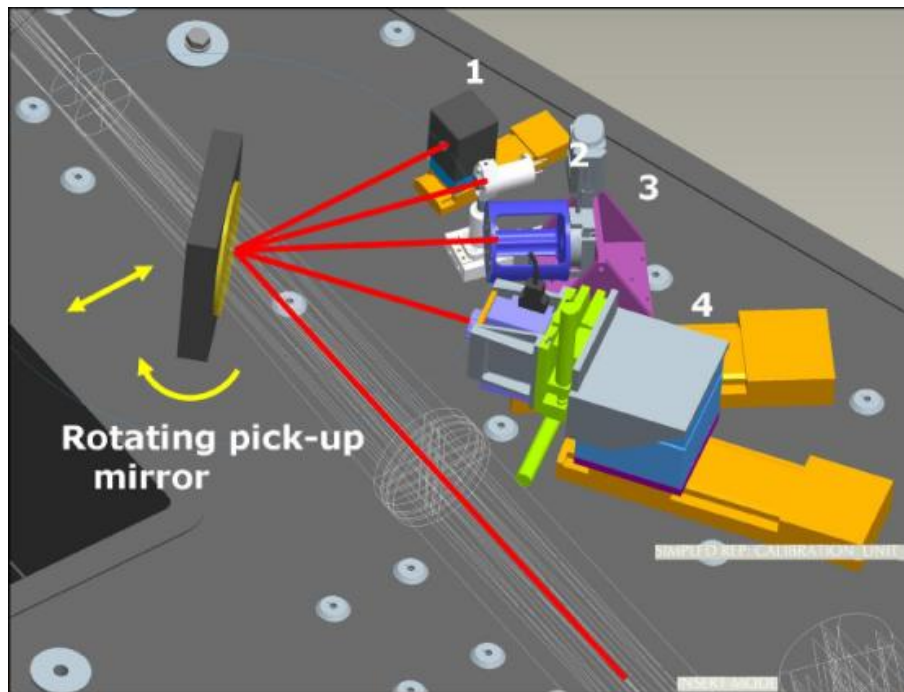


Figure 4. General view of the calibration unit

The pick-up mirror is also mounted on a translation stage used to insert and remove the mirror in the optical path, as represented by the double-arrow.

Four elements are present in the calibration unit and numbered as shown in Fig. 4:

- element #1: The fiber plate. This is the key element of the calibration unit. It supports the visible fibers for the DM and MHWS calibration, as well as the equalized fiber splitter for the zero-OPD calibration. Detailed description of this component is provided in Sect. 4.1.
- element #2: The phase diversity unit devoted to the calibration of the *non-common path aberrations*. See Sect. 4.2.
- element #3: The integrating sphere for the detector flat-field. See Sect. 4.3
- element #4: The Twyman-Green interferometer, also called *FISBA interferometer*, for purposes of general alignment. See Sect. 4.3.

#### 4.1. Fiber plate

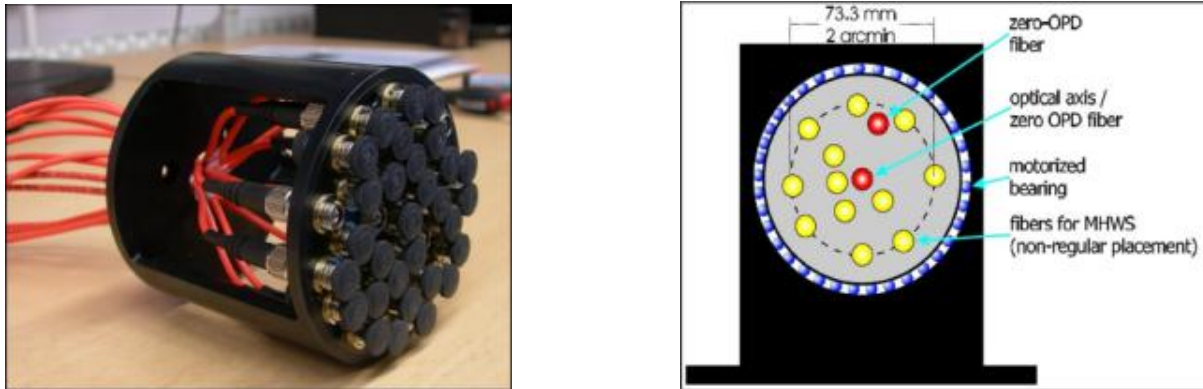


**Figure 5.** *Left:* Fiber plate hardware with mounted visible fibers. *Right:* concept of the fiber plate with the twelve MCAO calibration fibers and the two zero-OPD calibration fibers

The fiber plate supports a total of twelve optical fibers that simulate a reference star field for the eight pyramid wavefront sensor. The fiber arrangement reproduces the stellar field of  $2' \times 2'$  given a plate scale of  $600 \mu\text{m}/\text{arcsec}$ . In Fig. 5 is shown the piece of hardware that supports the fibers. Furthermore, the plate can be rotated around the optical axis thanks to the motorized bearing. This operation is required in order to ensure the complete illumination of the deformable mirrors. Eight fibers are mounted on the  $2'$  diameter circle and four additional fibers are mounted inside this circle.

The fiber plate supports also the two “zero-OPD” fibers for the interferometric calibration. The center one helps to calibrate the on-axis equality of the optical paths in each arm. The off-axis source is used to verify the homotheticity of the pupil: when this condition is fulfilled, the fringe pattern can be observed for both on-axis and off-axis positions. The zero-OPD fibers operate at  $1.3 \mu\text{m}$ . The core is unresolved, which simulates a point-like source.

The fibers for the MCAO calibration are connected to a fibered laser source at  $0.632 \mu\text{m}$ , while the zero-OPD fiber splitters are connected to a broadband source centered at  $1.3 \mu\text{m}$  with  $20 \mu\text{m}$  coherence length. The sources are located in a separate thermalized cabinet to avoid any hot point in the vicinity of the instrument, and connected to the individual components of the calibration unit thanks to 5-m to 10-m long singlemode fibers.

#### 4.2. The phase diversity unit

The principle of the method is presented in Sect. 3.1. Practically, we select a concept for which the in focus and out-of-focus images are obtained simultaneously thanks to a set of three fibers placed at the desired position in

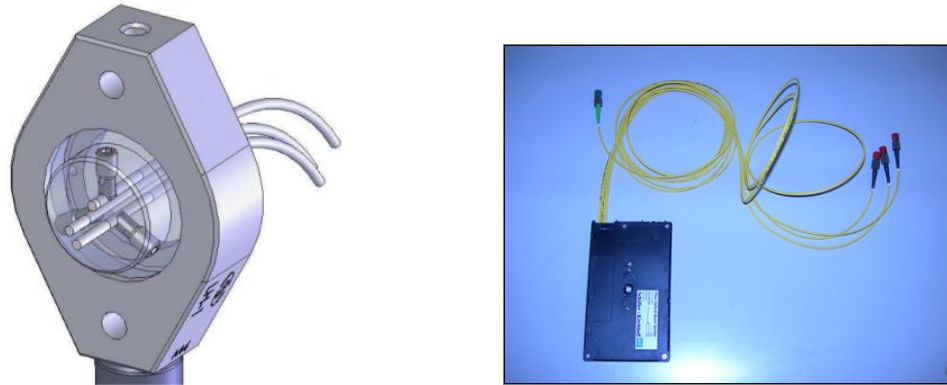


**Figure 6.** *Left:* Selected arrangement for the phase diversity concept on the calibration unit. *Right:* 1 to 3 beam splitter for the phase diversity calibration.

the telescope focal plane. Fig. 6, left, shows the selected arrangement of the three fibers with a relative shift of  $\pm 2.5$  mm. In principle, the in-focus and out-of-focus images should be taken through exactly the same optical path.<sup>2</sup> However, the numerical aperture of the fiber ensures that the illuminated regions of the lens are almost equal, and that the relative difference could be neglected for the analysis of the phase diversity method. The hardware used for the unit component is a 1 to 3 singlemode fiber splitter in the near-infrared at  $1.3 \mu\text{m}$  (see Fig. 6, right).

So far, we have conducted preliminary laboratory tests of the phase diversity algorithm written on IDL and previously used for the NCPA calibration on the NACO instrument.<sup>4</sup> The first results have shown that we can visually obtain a good agreement between the original PSF and the reconstructed one. However the direct comparison of the Zernike spectra between the experimental and reconstructed data shows several mismatches which are currently under investigation.

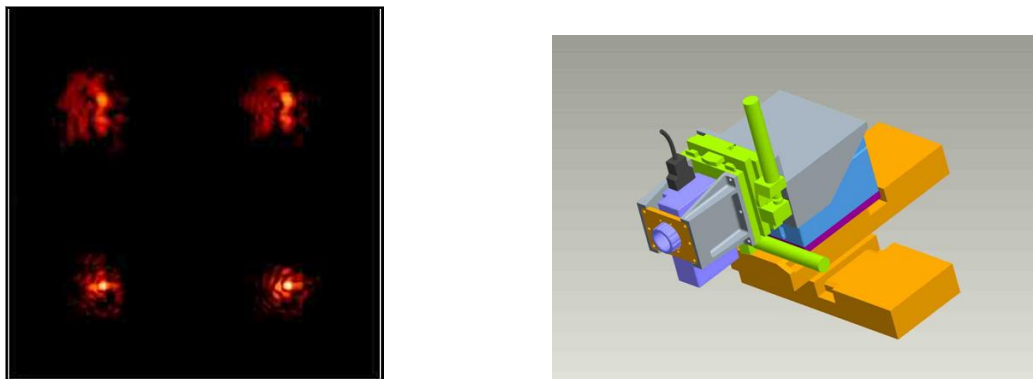


**Figure 7.** *Left:* Phase diversity outputs from lab experiment. Left column: experimental out-of-focus PSF (upper left corner) and in focus PSF (lower left corner). Right column: Reconstructed PSF using the phase diversity method. *Right:* Design of the FISBA interferometer unit, with tip-tilt and X-Y-Z stages.

### 4.3. Integrating sphere and Twyman-Green interferometer

The integrating sphere is the common calibration component to perform accurate flat-fields of the detector. We purchased an integrating sphere by the company *Sphere Optics* covering the J, H and K bands. The detector size in the telescope focal plane is  $6 \times 6$  mm considering the  $600 \mu\text{m}/\text{arcsec}$ . The requirement on the size of the sphere is that the area of the detector does not exceed 90% of the output port surface to obtain good uniformity of the detector illumination. This translates in a minimum diameter of the output port of 7.5 mm, or 0.3 inches. This led us to select the product SPH-2Z from *Sphere Optics*, which has 3 output ports with 12.7 mm diameter for a

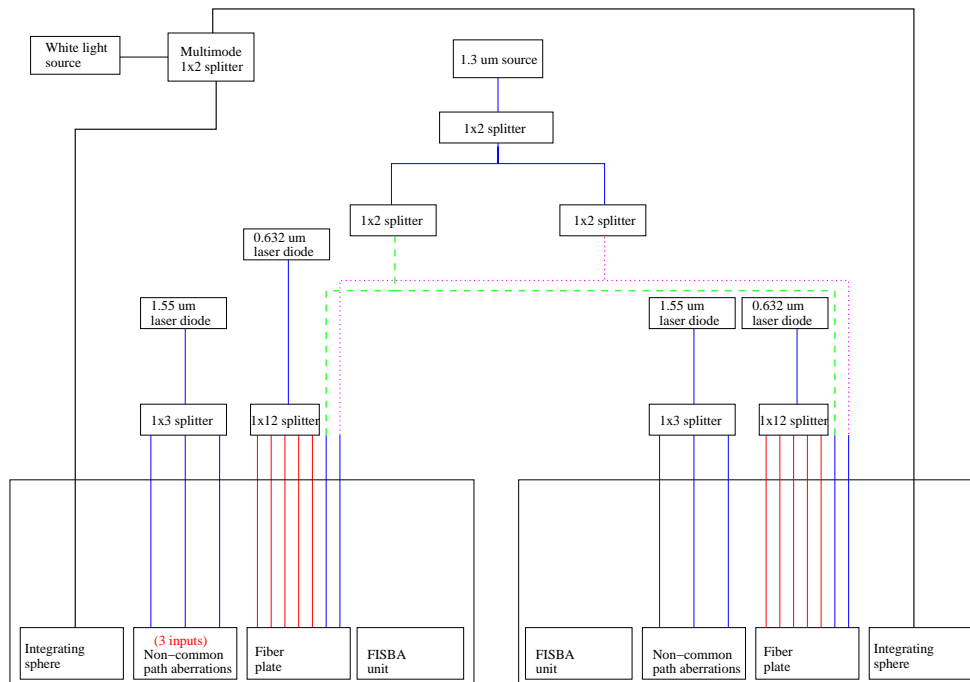


**Figure 8.** Functional diagram of the connecting system adopted for the two calibration units. The dashed and continuous lines represent the optical fibers and splitters. In this way, all the light sources are kept distant from the bench.

sphere diameter of 2 inches. The internal coating – named ZENITH – is optimized for visible and IR operation. An important aspect in operating the integrating sphere is that any stray light and temperature effects due to the lamp heating should be avoided. Thus, the lamp will not be inserted in the sphere, as it is usually done, but it will be connected to the sphere through a fiber bundle that star, which allows us to limit the impact of spurious light. The lamp will be installed in the LINC-NIRVANA cabinet, which is controlled in temperature.

The Twyman-Green interferometer – also named *FISBA* interferometer – is used for general alignment. It will thus be part of the calibration unit only during commissioning time, when the instrument is installed on the LBT. The space reserved for this component could be possibly used in the future to integrate an additional sub-unit upon request. The FISBA component is installed on a tip-tilt stage as well as on X-Y-Z stage for accurate positioning. The position requirements are provided in a previous section.

Fig. 8 shows the functional diagram of the connecting system for the various components of the two calibration units. Except for the FISBA interferometer, all the other components are connected via fibers to their respective light sources in order to minimize the risks of disturbance of the instrument.

## 5. FIRST LABORATORY VALIDATION

Among all the different components of the calibration unit presented above, the “zero-OPD” unit is the most demanding one in terms of requirements. In particular, the equalization of the two arms has to be done very accurately in order to obtain in phase outputs within the coherence length of the broad band source. This is translated in an equalization of the optical path with an accuracy better than  $20 \mu\text{m}$ . The equalization is done by iteratively polishing the fibers arms and measuring their length. The experimental method to measure the differential OPD is based on the measurement of the relative position of the fringe packet position at outputs A and B of a Michelson type interferometer (see Fig. 9, left). The two mirrors are replaced with an optical system that permits us to inject the light from the broad band source into each arm of the splitter. At the level of the two arms outputs, labeled A and B, part of the light is reflected back by the fiber surface and part of the light is transmitted through the splitter to detector B. One of the injection optics system is placed on a

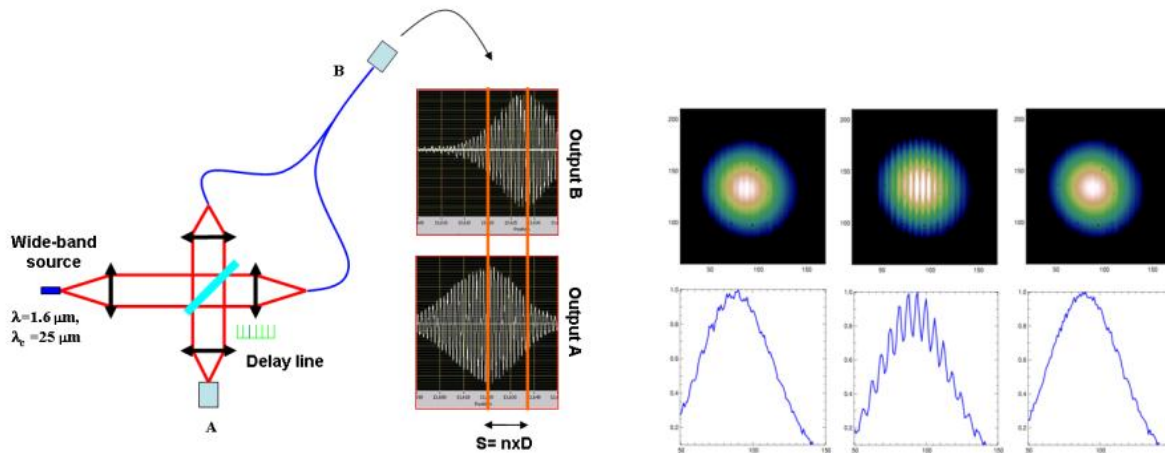


**Figure 9.** *Left:* Phase diversity outputs from lab experiment. *Left:* experimental out-of-focus PSF (upper left corner) and in focus PSF (lower left corner). *Right:* Reconstructed PSF using the phase diversity method.

delay line that can be translated with better than  $1\text{-}\mu\text{m}$  accuracy. By scanning the OPD over a sufficient long distance, two interferograms are measured on detector A and B. The fringe packet on detector A corresponds to the interferences between the beams back-reflected at the surface of the splitter output fibers. The fringe packet at detector B corresponds to the interferences between the recombined beams coupled into the splitter. Since it is possible to measure the absolute position of the fringe packet center with micron accuracy, the differential length between the two arms can be deduced. Depending also on the relative position between the two fringe packets, one can infer which arm is longer. Thus, by an iterative process of polishing and length measurement, one can reach the optical path equalization with an accuracy of  $5\ \mu\text{m}$ . Note that the relative positions of the fringe packet measure the optical path  $n \times D$ , where  $n$  is the refractive index and  $D$  the geometrical length. For a typical index  $n=1.5$  for silica fibers, the accuracy on the geometrical differential length is of the order of  $3.5\ \mu\text{m}$ . The interferograms of Fig. 9 show the results that were obtained on the equalization of our splitter. At the end of the iterative process previously described, the first fringe packet was measured with the delay line at an absolute position of  $13.620\ \text{mm}$ . The second fringe packet was measured at an absolute position of  $13.627\ \text{mm}$ , which leads to a differential geometrical length of  $\sim 7\ \mu\text{m}$ . We consider that such an accuracy is acceptable for our objectives and that the equalization method is valid. This operation is achieved in collaboration with the Laboratoire d'Astrophysique de Grenoble.

We also have tested in the lab the stability of the obtained fringes over a sufficient long period of time of circa three weeks. The plots of Fig. 9, right show the fringes obtained within the  $20\ \mu\text{m}$  coherence length of the source. The goal of this test was to detect potential long term differential elongation between the two arms. Once the fringes were obtained with our 2-m long fiber splitter, they could be maintained steadily over a period of three weeks. After this period, the experiment was stopped, but we are confident that a longer period could have been successfully probed.

On a short term perspective, we foresee the development of a new experiment to be installed directly on the LINC-NIRVANA bench. The experiment aims at mounting the final fiber splitter – 10 m total length – on its quasi-final configuration. The objective is to monitor the evolution of the differential OPD when the system undergoes flexure constraints. The LN bench can be tilted during integration to test the effects of flexure on the different sub-systems.

## REFERENCES

1. R. G. Paxman, T. J. Schulz, and J. R. Fienup, "Joint estimation of object and aberrations by using phase diversity," *Journal of the Optical Society of America A* **9**, pp. 1072–1085, 1992.
2. M. Hartung, A. Blanc, T. Fusco, F. Lacombe, L. Mugnier, G. Rousset, and R. Lenzen, "Calibration of naos and conica static aberrations. experimental results," *A&A* **399**, pp. 385–394, 2003.

3. A. Blanc, T. Fusco, M. Hartung, L. Mugnier, and G. Rousset, "Calibration of naos and conica static aberrations. application of the phase diversity technique," *A&A* **399**, pp. 373–383, 2003.
4. J. Kolb, "Eliminating the static aberrations in an mcao system," in *Advances in Adaptive Optics II*, B. L. Ellerbroek, ed., *Proc. SPIE* **6272**, p. 627258, 2006.